Implementation and Exploration of Parameterizations of Large-Scale Dynamics in NCAR's Single Column Atmosphere Model SCAM6

S. Cohen[1], A. Sobel[1], M. Biasutti[1], S. Wang[2], I. Simpson[3], A. Gettelman[3,4], and I. Hu[5,6]

[1] Columbia University, New York, NY, USA

[2] Nanjing University, Nanjing, Jiangsu, China

[3] National Center for Atmospheric Research, Boulder, CO, USA

[4] Pacific Northwest National Laboratory, Richland, WA, USA

[5] CIRES, University of Colorado, Boulder, CO, USA

[6] Physical Sciences Laboratory, NOAA, Boulder, CO, USA

Corresponding author: Sean Cohen (sean.cohen@columbia.edu)

Key Points:

- We use three different methods to parameterize the large-scale dynamics in NCAR's single column atmospheric model (SCAM6).
- As in the Global Atmospheric System Studies Intercomparison, we test SCAM6's response to various boundary conditions and model parameters.
- Under all three methods, circulation strength is decreased when barriers to convection are reduced.

Abstract

A single column model with parameterized large-scale dynamics is used to better understand the response of steady-state tropical precipitation to relative sea surface temperature under various representations of radiation, convection, and circulation. The large-scale dynamics are parametrized via the weak temperature gradient (WTG), damped gravity wave (DGW), and spectral weak temperature gradient (Spectral WTG) method in NCAR's Single Column Atmosphere Model (SCAM6). Radiative cooling is either specified or interactive, and the convective parameterization is run using two different values of a parameter that controls the degree of convective inhibition. Results are interpreted in the context of the Global Atmospheric System Studies (GASS) Intercomparison (Daleu et al. 2016). Using the settings given in Daleu et al. (2016), SCAM6 under the WTG and DGW methods produces erratic results, suggestive of numerical instability. However, when key parameters are changed to weaken the strength with which the circulation acts to eliminate tropospheric temperature variations, SCAM6 performs comparably to single column models in the GASS Intercomparison. The Spectral WTG method is less sensitive to changes in convection and radiation than are the other two methods, performing at least qualitatively similarly across all configurations considered. Under all three methods, circulation strength, represented in 1D by grid-scale vertical velocity, is decreased when barriers to convection are reduced. This effect is most extreme under specified radiative cooling, and is shown to come from increased static stability in the column's reference radiative-convective equilibrium profile. This argument can be extended to interactive radiation cases as well, though perhaps less conclusively.

Plain Language Summary

Single column models, as the name suggests, only model the vertical dimension of the atmosphere. They are simpler than full-scale 3D global circulation models, but nonetheless play an important role in model development and in better understanding physical phenomena. We use NCAR's Single Column Atmosphere Model (SCAM6) to better understand tropical rainfall. In a single column model, the atmospheric wind coming from other locations (the large-scale circulation) must be either specified or approximated using a parameterization. We implement three different parameterizations of the large-scale circulation into SCAM6 and assess how SCAM6 responds to various changes while using these parameterizations. The Global Atmospheric System Studies (GASS) Intercomparison assessed the performance of various other single column models using parameterizations of the large-scale circulation; we fold SCAM6 into this Intercomparison. We find that SCAM6 performs substantially differently to its peers under the settings used in the GASS Intercomparison, but more comparably to its peers when key circulation parameters are relaxed. Another notable finding is that, across all three parameterizations of large-scale dynamics, circulation strength decreases when we reduce SCAM6's barrier to convection.

1 Introduction

Single column models (SCMs) are one-dimensional (1D) models that only explicitly represent the vertical dimension of the atmosphere. While the column's full convective, radiative, and moist physics schemes are retained, the large-scale dynamics must be either specified or parameterized. While SCMs only represent a subset of the processes captured in full-scale 3D global circulation models (GCMs), they are part of model hierarchies which can play important roles both in model development and in better understanding underlying physical phenomena (Held 2005).

Parameterizations of the large-scale dynamics are best developed in the context of the tropical atmosphere. Due to the smallness of the Coriolis parameter near the equator, tropical horizontal free-tropospheric pressure and density gradients are weak on climatic time scales (Charney 1963). For some purposes, it can be assumed that large-scale dynamics will simply act to relax the column's temperature to a predefined profile representative of regions adjacent to the column, and by extension the tropics as a whole. This target profile is often modeled as a radiative convective equilibrium (RCE) solution over an appropriate sea surface temperature, representing either the tropical mean or the mean over regions of frequent deep convection (Sobel and Bretherton 2000, Sobel et al. 2002). In RCE, the large-scale vertical velocity is zero, meaning that radiative cooling balances convective heating at all pressure levels and column precipitation must equal column evaporation. Any given region within the tropics can sustain precipitation greater or less than the tropical mean by importing or exporting moisture via the large-scale circulation. Parametrizations of large-scale dynamics try to capture this process, including its dependence on both external parameters (e.g., local sea surface temperature) and internal ones (e.g., those that represent aspects of convective or radiative physics).

The goal of this paper is to test several parameterizations of large-scale dynamics in NCAR's Single Column Atmosphere Model, SCAM6 (Gettelman et al. 2019), the SCM version of NCAR's Community Earth System Model, CESM2.2.0 (Danabasoglu et al. 2020). SCAM6 retains the full radiation, convection, and other physics schemes included in CESM2.2.0, but requires the large-scale circulation to be either specified or parameterized. We parameterize the circulation via the following methods: the weak temperature gradient (WTG) method (Raymond and Zeng 2005), damped gravity wave (DGW) method (Kuang 2008), and the spectral weak temperature gradient (Spectral WTG) method (Herman and Raymond 2014, Wang et al. 2016).

These parameterizations of large-scale dynamics have been implemented into various SCMs and cloud resolving models (CRMs). To date, the most comprehensive analysis of how the WTG and DGW methods perform across SCMs and CRMs is the Global Atmospheric Systems Study (GASS) WTG Intercomparison, which assessed the steady-state response of twelve models in precipitation, moisture, temperature, and circulation strength to changes in relative SST, i.e., varying SST while holding the target tropospheric temperature profile fixed (Daleu et al. 2015, 2016) using both WTG and DGW (but not Spectral WTG). One goal of this study is to fold NCAR's Single Column Atmospheric Model SCAM6 into the results of the GASS Intercomparison study by implementing the same parameterizations of large-scale dynamics into SCAM6 and replicating the conditions applied by Daleu et al. (2016). It will also assess how the Spectral WTG method compares to the WTG and DGW methods in SCAM6, and analyze how the circulation responds to changes to the radiative and convective scheme. Since SCAM6 is primarily a tool for model development (Gettelman et al. 2019), this study's idealized simulations may also serve to inform future development of CESM.

Under the conditions applied in the GASS Intercomparison study, the WTG and DGW methods produce erratic results, suggestive of numerical instability (see Results). Thus, we alter key parameters in the methods to improve performance and subsequently present four different configurations of the convection and radiation schemes in SCAM6: 1) specified radiation with inhibited convection (RsCi), 2) specified radiation with uninhibited convection (RsCu), 3) interactive radiation with inhibited convection (RiCi), 4) interactive radiation with uninhibited convection (RiCu). Specifically in this study, idealized radiation refers to the radiative cooling profile used in Daleu et al. (2016) and modeled radiation refers to the default radiation package in SCAM6. Likewise, "inhibited" and "uninhibited" convection refer to different values of a parameter in SCAM6's deep convection scheme that controls the number of model levels over which a rising parcel can experience negative buoyancy before deep convection is suppressed, a parameter shown to have important effects in RCE simulations by Hu et al. (2022). We include specified radiation cases for better comparison between SCAM6 and the SCMs in Daleu et al. (2016), and we include interactive radiation cases for better assessment of the overall performance of SCAM6 under parameterized large-scale dynamics and of the interaction between its radiation and convection schemes.

This paper is organized as follows. The Methods section both describes the details of each parameterization implemented into SCAM6 (WTG, DGW, and Spectral WTG) as well as outlines the model set up and each of the four different configurations of the convection and radiation schemes (RsCi, RsCu, RiCi, and RiCu). The Results section discusses the performance of each parameterization under the conditions given in Daleu et al. (2016) and, once key circulation parameters are relaxed, under each of four different radiative and convective configurations. The Discussion section presents key takeaways regarding the relative performance of each parameterization of large-scale dynamics under the configurations considered and regarding important mechanistic feedbacks between the circulation, convection and radiation schemes. Finally, the Conclusion section summarizes the study and assesses its relevance to NCAR's GCM CESM2.2.0 and to tropical precipitation more broadly.

2 Methods

2.1 Parameterizations of Large-Scale Dynamics

This study considers three parameterizations of large-scale dynamics: the weak temperature gradient (WTG) method (Sobel and Bretherton 2000, Raymond and Zeng 2005), the damped gravity wave (DGW) method (Kuang 2008, Kuang 2011), and the spectral weak temperature gradient (Spectral WTG) method (Herman and Raymond 2014, Wang et al. 2016).

In the weak temperature gradient (WTG) method, we neglect the horizontal advection and time dependent terms from the column's temperature equation, and represent adiabatic warming or cooling due to vertical motion by a Newtonian relaxation of the virtual potential temperature in the column, $\overline{\theta_v}$, back to the target profile, $\overline{\theta_v^{ref}}$, on a time scale, τ. The vertical velocity, $\overline{\omega}$, is then diagnosed according to Raymond and Zeng 2005:

$$\overline{\omega}\frac{\partial\overline{\theta_v}}{\partial p} = \frac{\left(\overline{\theta_v} - \overline{\theta_v^{ref}}\right)}{\tau}$$

The WTG approximation breaks down in the boundary layer due to the effects of surface turbulent fluxes of heat and momentum. The pressure vertical velocity ought to vanish at the surface in steady state, so we linearly interpolate $\overline{\omega}$ from its WTG value at 850 Pa to zero at the surface, as is done in Daleu et al. (2016). In addition, to avoid numerical issues, we place a lower limit of 2e^{-4} K Pa^{-1} on the absolute value of the static stability, $\frac{\partial \overline{\theta_v}}{\partial p}$ (Raymond and Zeng 2005), used in the calculation of $\overline{\omega}$.

The DGW method attempts to more explicitly capture the gravity wave dynamics that act to relax the column back to the tropical mean. Using the 2D anelastic nonrotational momentum, continuity, and hydrostatic equations, the DGW method applies a wave equation for $\overline{\omega}$. At each time step, a single linear gravity wave of specified horizontal wave number, k, minimizes deviations in virtual temperature, $\overline{T_v}$, from the target profile, $\overline{T_v^{ref}}$ (Kuang 2008, Kuang 2011):

$$\frac{\partial}{\partial p}\left(\epsilon \frac{\partial \overline{\omega}}{\partial p}\right) = \frac{k^2 R_D}{\overline{p^{ref}}}\left(\overline{T_v} - \overline{T_v^{ref}}\right)$$

Here, R_D is the gas constant of dry air and ϵ is the specified mechanical damping coefficient. We exclude the time derivative on the left-hand side since we are primarily concerned with the column's steady state response. We apply homogeneous boundary conditions for $\overline{\omega}$ at the surface and at a nominal upper boundary (100 hPa), and solve the wave equation at each time step using a standard triangular matrix solver. As in Daleu et al. (2016), we set the horizontal wavenumber, k, to 10^{-6} m^{-1}, corresponding to a wavelength of about 6000 km.

The spectral WTG method also uses gravity wave dynamics to more accurately capture the large-scale relaxation to the target temperature profile. Recognizing that gravity waves of different wavelengths will travel at different speeds, the spectral WTG method damps each spectral mode's temperature forcing proportionally to that mode's theoretical gravity wave speed (Herman and Raymond 2014). Following Wang et al. (2016), who used a slightly different approximation than Herman and Raymond (2014), we derive these spectral modes and their corresponding theoretical wave speeds by constructing an equation for the vertical velocity, again assuming a 2D non-rotating anelastic atmosphere. Homogeneous boundary conditions enforce that the vertical velocity vanish at the surface and at the tropopause, and Boussinesq-like assumptions eliminate any single derivatives in $\overline{\omega}$:

$$(\rho \overline{w})_{zz} + \frac{N^2}{c^2}(\rho \overline{w}) = 0$$

Note that the vertical velocity, $\overline{w}$, is now in height, not pressure coordinates. For constant Brunt-Vaisala frequency, N, each mode will be sinusoidal and its corresponding wave speed can be diagnosed from its eigenvalue. We project the usual WTG forcing onto these modes, but the damping time constant, τ_n, of each nth mode varies according to its wave speed, c_n. Since c_n is inversely proportional to n, the gravest spectral mode is damped most quickly, while modes associated with larger n are damped more slowly, yielding:

$$\rho \overline{w} = \sum_{n=1}^{\infty} \frac{A_n}{n} \sin\left(\frac{n\pi z}{H}\right)$$

$$A_n = \frac{2}{H}\int_0^H \frac{\left(\overline{\theta_v} - \overline{\theta_v^{ref}}\right)}{\left(\frac{\partial \overline{\theta_v}}{\partial z}\right)\tau_1} \sin\left(\frac{n\pi z}{H}\right) dz$$

Here, H is the specified height of the tropopause, A_n is the normalized projection of the WTG forcing onto the spectral modes, and τ_1 is the damping time constant of the first, or gravest, mode. Since modes of larger n will generally have smaller magnitude due to the linear scaling of τ_n with n, we numerically implement the Spectral WTG method by considering only the first twenty terms of the infinite series, with negligible truncation error (not shown). As with the WTG method, we place a lower limit of 2e^{-4} K Pa^{-1} on the absolute value of the static stability, $\frac{\partial \overline{\theta_v}}{\partial p}$.

2.2 Model Configuration

The WTG, DGW, and Spectral WTG methods all require some choice of a reference tropical temperature profile. Since circulation implies the horizontal advection of moisture (discussed in more detail below), we must also determine a reference mean tropical moisture profile. To replicate the setup used in Daleu et al. (2016), we calculate the reference temperature and moisture profiles by running SCAM6 in RCE (i.e. imposing zero vertical velocity) for uniform 300K sea surface temperature (SST), a value intended to be representative of the tropical average. Starting from a moist adiabatic temperature profile with uniform 70% relative humidity, we run SCAM6 in RCE for 300 days and average over the final 100 days. In any runs that explore different convection and radiation schemes, we also use these settings to generate distinct RCE reference temperature and moisture profiles to ensure consistency between the modeled column and the reference mean tropical state. In all cases, horizontal wind speed is set to a vertically uniform value of 5 m s^{-1}, a prescription which does not affect the dynamics of convection, but plays an important role in computing surface fluxes (Daleu et al. 2015, 2016). All RCE reference profiles assume 300K SST.

As in Daleu et al. (2016), this study assumes no horizontal advection of temperature, so that the temperature ($\overline{\theta_v}$) tendency can be written as:

$$\left(\frac{\partial \overline{\theta_v}}{\partial t}\right)_{LS} = -\overline{\omega}\frac{\partial \overline{\theta_v}}{\partial p}$$

Moisture ($\overline{q_v}$) is treated differently and instead is subject to a one-way "lateral entrainment" described by Raymond and Zeng (2005). In addition to vertical advection by $\overline{\omega}$, moisture is horizontally advected into the column by local flow convergence, yet is not altered at levels of local flow divergence:

$$\left(\frac{\partial \overline{q_v}}{\partial t}\right)_{LS} = -\overline{\omega}\frac{\partial \overline{q_v}}{\partial p} + max\left(\frac{\partial \overline{\omega}}{\partial p}, 0\right)\left(\overline{q_v^{ref}} - \overline{q_v}\right)$$

While some studies represent the horizontal advection of moisture differently (Sobel et al. 2007, Sobel and Bellon 2009, Wang and Sobel 2012), Daleu et al. (2016) and many other studies

(Raymond and Sessions 2007, Sessions et al. 2010, Wang et al. 2013, Herman and Raymond 2014) use this "lateral entrainment" of moisture.

Daleu et al. (2016) specifies an idealized radiative cooling profile to isolate interactions between convection and large-scale dynamics in each model. They prescribe a uniform 1.5 K day^{-1} cooling rate below 200 hPa, relax the temperature above 100 hPa to 200 K, and linearly interpolate between these cooling rates between 100 hPa and 200 hPa:

$$\left(\frac{\partial T}{\partial t}\right)_{RC} = \begin{cases} -1.5 & if\ \bar{p} \geq 200 \\ -1.5\left(\frac{\bar{p}-100}{100}\right) - \alpha_T\left(\frac{200-\bar{p}}{100}\right)(\bar{T}-200) & if\ 100 < \bar{p} < 200 \\ -\alpha_T(\bar{T}-200) & if\ \bar{p} \leq 100 \end{cases}$$

They set the constant α_T to 1 day^{-1}. For this study, we run cases using either the specified radiation above or the interactive radiation package in SCAM6, a streamlined version of the rapid radiative transfer method (RRTMG) that derives from a correlated k-distribution (Lacis et al. 1979). We refer to cases run using specified radiation with the label "Rs" and refer to cases run using RRTMG, or fully interactive radiation, with the label "Ri".

SCAM6 uses a unified turbulence scheme, Cloud Layers Unified by Binormals (CLUBB), for shallow convection (Golaz et al. 2002) and the Zhang-McFarlane (ZM) scheme (Zhang and McFarlane 1995) for deep convection. The ZM scheme allows an ensemble of convective-scale updrafts, and associated saturated downdrafts, to occur whenever the lower troposphere is conditionally unstable and the updrafts have sufficient buoyancy to penetrate the stable layer. These updrafts act to consume convective available potential energy (CAPE) in the convective layer at a specified time scale (two hours).

One of the critical parameters in SCAM6's version of the ZM scheme is *zmconv_num_cin*, renamed δ_{CIN} for this study, which specifies the number of negative buoyancy levels that are allowed before the convective layer is capped and CAPE calculations are completed. This parameter determines the scheme's ability to overcome some amount of convective inhibition (CIN), which in turn often determines the level of convective cloud top. The default value of δ_{CIN} for SCAM6 is one, which sets the lowest neutral-buoyancy level of a pilot entraining plume to be the convective cloud top. This choice tends to cause the model to underestimate tropical variability and convective cloud top in global simulations (Xie et al. 2018, Wang and Zhang 2018) and produces a shallow-convection prevailing regime in an idealized RCE framework (Hu et al. 2022). The default value of δ_{CIN} for SCAM6 is therefore being changed to three in future versions of CESM (personal communication). Thus, for this study we run cases using either $\delta_{CIN} = 1$, referred to as inhibited convection (Ci), or $\delta_{CIN} = 3$, referred to as uninhibited convection (Cu).

Finally, each of the parameterizations of large-scale dynamics contain parameters that specify the strength of the circulation response to a given temperature anomaly. In the WTG and Spectral WTG methods, τ and τ_1 set the time scale at which the column's temperature and the gravest spectral mode of the column's temperature, respectively, are relaxed back to the tropical mean. In the DGW method, ϵ plays a similar role, setting the mechanical damping coefficient with which the gravity waves are damped, notwithstanding that its units are the inverse of those of τ.

The specified horizontal wave number, k, also plays a significant role in setting the strength of the circulation response, though this is left constant in the present study. Daleu et al. (2016) sets τ to 3 hours and ϵ to 1 day^{-1}. These are typical values used in previous studies (Herman and Raymond 2014, Daleu et al. 2012, Wang and Sobel 2011, Wang et al. 2013) and are chosen to produce comparable circulation responses to the same free tropospheric temperature anomaly in both methods. In the present study, we take the circulation parameter values given in Daleu et al. (2016) as a starting point, and increase or decrease them to weaken or strengthen the circulation response. The WTG and DGW methods in SCAM6 are led to erratic behavior, suggestive of numerical instability, for the default values of τ and ϵ used in Daleu et al. (2016), perhaps due to the ZM convection scheme. For τ = 3 hours, the WTG method yields vertical velocity and convective heating profiles that oscillate wildly, and, for ϵ = 1 day^{-1}, the DGW method both crashes at 298K SST and yields unrealistic S-shaped vertical velocity profiles at other values of SST (see Results). Thus, we increase τ and ϵ three- or five-fold from the Daleu et al. (2016) values for most cases presented. While the Spectral WTG method tends to be robust even at lower values of τ_1, we match τ_1 to τ in all cases considered.

We run all cases using parameterized large-scale dynamics for 400 days under constant SST values of 298 K, 299 K, 300 K, 301 K, and 302 K. This range of SST values is comparable to the range used in Daleu et al. (2016). We find the steady-state precipitation, evaporation, vertical velocity, relative humidity, temperature anomaly, and convective and radiative heating rates by averaging the final 100 days of the run. All runs presented in this study use twenty-minute time steps and 32 pressure levels. Several cases were also run using sixty pressure levels, though we observed no significant change in results under this increased vertical resolution. Some runs, especially for lower values of δ_{CIN}, τ, and ϵ, demonstrate multiple quasi steady-state equilibria. In all cases where we observe such behavior, we extend the run an additional 400 days to ensure no sizable variations occur in the steady-state quantities considered. We leave further exploration of such transient phenomena to future study. It is also worth mentioning that, in cases of interactive radiation (Ri), there is a seasonal cycle of insolation equivalent to that seen at the equator. However, when averaged over 365 days rather than 400 days, there is no significant change in any output parameters.

3 Results

3.1 Radiative-Convective Equilibrium

To begin, we consider the reference RCE state for each model configuration. We present quantities of interest from these RCE states in Table 1, which displays time-averaged precipitation and evaporation, and Figure 1, which displays time-averaged temperature, relative humidity, and radiative and convective heating profiles.

By design, the precipitation and evaporation in RCE are nearly identical (Table 1). The choice of specified vs. interactive radiation scheme causes large differences in the time-averaged precipitation and evaporation; this is unsurprising given that the idealized radiative cooling profile in Daleu et al. (2016) implies a substantially larger vertically integrated cooling than the interactive scheme computes under these conditions, and this integrated cooling must be balanced by the sum of condensation heating and sensible surface heat flux in RCE. Differences in convection affect precipitation not at all for the interactive radiation cases and only slightly for the idealized radiation cases (less than 10%). Since we specify radiative cooling, and thus convective heating, to be 1.5 K day^{-1} below 200 hPa in the idealized radiation configuration, the changes appear to be primarily the result of relatively large upper tropospheric (above 200hPa) temperature differences (Figure 1). Deep convection happens more easily when δ_{CIN} is set to 3, meaning the upper troposphere is substantially warmer in this case, yielding greater radiative cooling, which is balanced with greater precipitation.

Precipitation (Evaporation)	Inhibited Convection (Ci)	Uninhibited Convection (Cu)
Interactive Radiation (Ri)	2.74 (2.72)	2.74 (2.74)
Specified Radiation (Rs)	4.29 (4.30)	4.57 (4.58)

Table 1. Precipitation and evaporation (mm/day) in RCE for each convective and radiative setting considered. Ri indicates use of the default interactive radiation scheme in SCAM6, Rs indicates use of specified radiative cooling, Ci indicates 1 level of CIN is tolerated in the convection scheme, and Cu indicates 3 levels of CIN are tolerated in the convection scheme.

The far-left plot in Figure 1 shows the time-averaged RCE temperature profile in SCAM6 for the radiative and convective conditions used in GASS (RsCi, black dotted line). The subsequent plots in Figure 1 show (left to right) the deviation of each RCE temperature profile from RsCi, the relative humidity profile, the radiative cooling profile, and the convective heating profile for RsCi, RsCu, RiCi, and RiCu (black dotted line, black solid line, blue dotted line, and blue solid line, respectively). All profiles are time-averaged. One standard deviation in time (gray shaded area) is shown for RiCu; variances for other cases are similar in magnitude, save of course the radiative cooling profile in Rs cases which is specified. On the whole, the idealized radiation configuration yields a cooler troposphere than the interactive radiation case, likely because the specified 1.5 K day^{-1} radiative cooling rate below 200 hPa is larger than what the interactive radiation scheme predicts for nearly all pressure levels (Figure 1). Relative humidity (RH) is computed with respect to liquid water and remains between 50% and 80% throughout the free troposphere for all RCE cases except the specified radiation with uninhibited convection case (RsCu), which shows substantially less moisture in the mid troposphere.

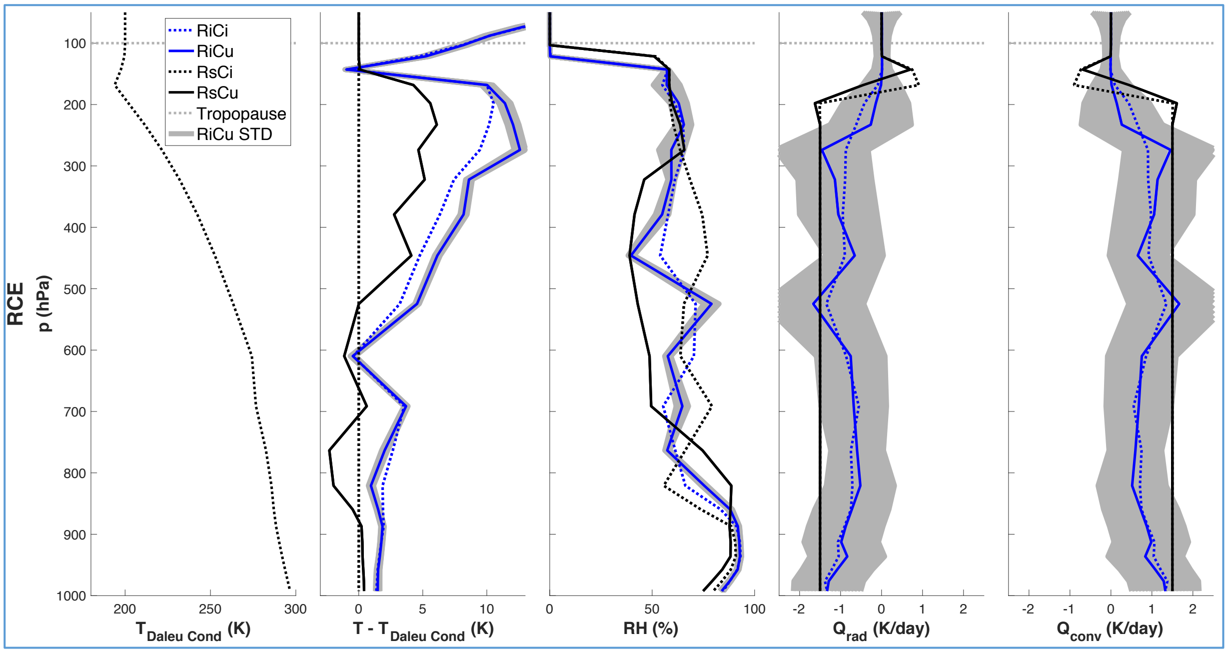

Figure 1. Column temperature, relative humidity, and convective and radiative heating in RCE for each convective and radiative setting considered. Ri indicates use of the default interactive radiation scheme in SCAM6, Rs indicates use of specified radiative cooling, Ci indicates 1 level of CIN is tolerated in the convection scheme, and Cu indicates 3 levels of CIN are tolerated in the convection scheme. The subscript "Daleu Cond" indicates use of all conditions given in Daleu et al. 2015/2016, or RsCi. For reference, one standard deviation of model output over the last 100 days is shown for the RiCu case. The tropopause (100 hPa) is shown in dashed gray.

3.2 Parameterized Large-Scale Dynamics Under GASS Settings

We then simulate a column state in response to cooler and warmer SSTs than the reference 300K RCE value (298K, 299K, 300K, 301K, and 302K), holding the above RCE temperature and moisture profiles fixed as reference states for each of the parameterizations of large-scale dynamics. We first consider the RsCi case as a way to directly compare SCAM6 with Daleu et al. (2016). We also set the circulation parameters to the values given in Daleu et al. (2016), with τ_1 and τ set to 3 hours and ϵ set to 1 day^{-1}. Results are shown in Figure 2.

Under the WTG approximation, we expect a positive, monotonic relationship between SST and precipitation (Sobel and Bretherton 2000). Lower-than-average SSTs should yield large-scale descent that suppresses convection, dries out the free troposphere, and allows relatively little precipitation. By contrast, higher SSTs should yield large-scale ascent that enhances convection, moistens the free troposphere, and generates relatively heavy precipitation. In Figure 2, we check this expectation by plotting precipitation (blue) and evaporation (red) as a function of SST. While the Spectral WTG method performs as expected, the WTG and DGW methods not only do not follow this expectation, but also demonstrate erratic behavior suggestive of numerical instability. This is shown in the simulated profiles of vertical velocity, temperature deviation from RCE, radiative cooling, convective heating, and relative humidity for each method at each SST (Figure 2, colors scale from cool to warm). In the WTG method, both the vertical velocity and convective heating oscillate wildly, with the substantial variations in SST showing little effect on the solution. While the runs using the DGW method behave a bit less erratically, there are clear numerical issues in the upper troposphere and again few if any interpretable results (this result is robust across all rigid lid DGW simulations, even when the height of the rigid lid is varied from 200 to 10 hPa). Additionally, the DGW method crashes at 298 K SST for this configuration, so no data is shown for this run.

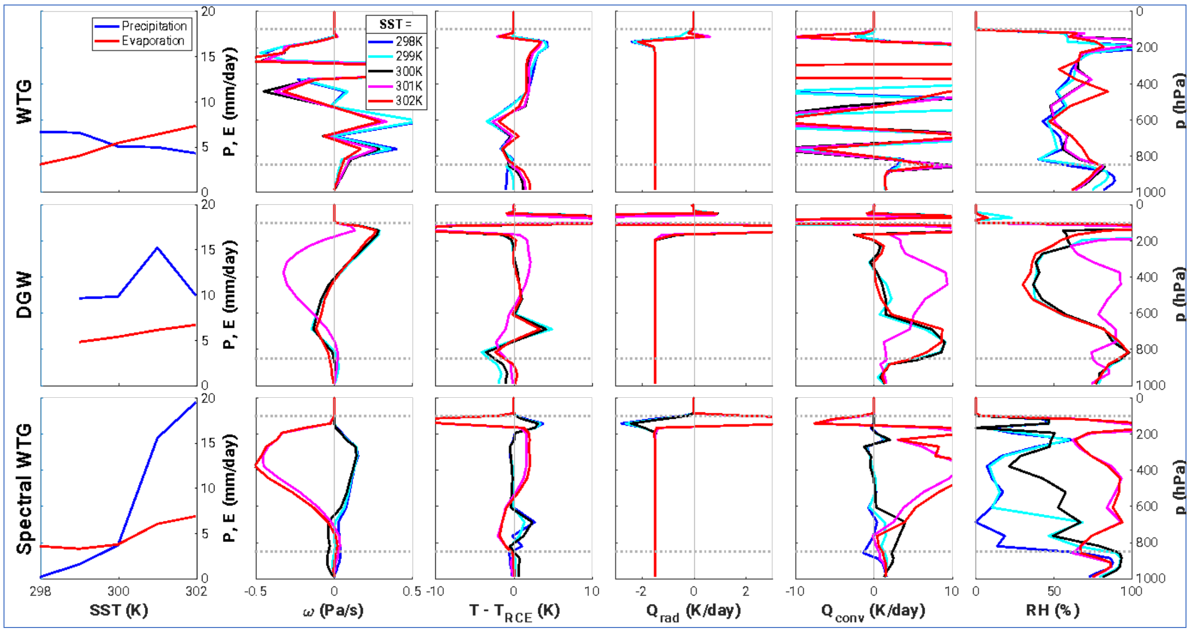

Figure 2. RsCi: Steady-state precipitation, evaporation, vertical velocity, temperature anomaly, relative humidity, and convective and radiative heating in WTG, DGW, and Spectral WTG for τ_1 and τ set to three hours and ϵ set to one day^{-1} using specified radiative cooling and tolerating one level of CIN in the convection scheme. The tropopause and boundary layer height are shown in dashed gray. Note that different scales are used for convective and radiative heating rates.

3.3 Parameterized Large-Scale Dynamics Under Relaxed Settings

If we increase the parameters used in Daleu et al. (2016) to weaken the strength of the circulation response, the WTG and DGW methods perform more reasonably. This is shown in Figure 3, which presents runs using three times the circulation parameters given in Daleu et al. (2016), with τ_1 and τ set to nine hours and ϵ set to three days^{-1}. Radiative and convective settings are left unmodified (RsCi). Increasing τ, τ_1, and ϵ weakens the circulation response to a given temperature perturbation from the tropical mean, which has the effect of smoothing the vertical velocity profiles. The WTG method (top) behaves more consistently with expectations; low SSTs yield gentle large-scale descent and light precipitation while high SSTs yield strong large-scale ascent and heavy precipitation. Qualitatively, the WTG method performs similarly to the Spectral WTG method for this configuration. However, the Spectral WTG method is able to sustain larger magnitude large-scale ascent for higher SSTs, making its steady-state precipitation for these runs substantially larger. The DGW method yields exceptionally dry conditions in this configuration, where the expected deep convection and heavy precipitation for higher SST is not observed. It is also worth noting that some grid-scale oscillation is observed for low SST runs in the upper tropospheric relative humidity profiles of the DGW and Spectral WTG methods.

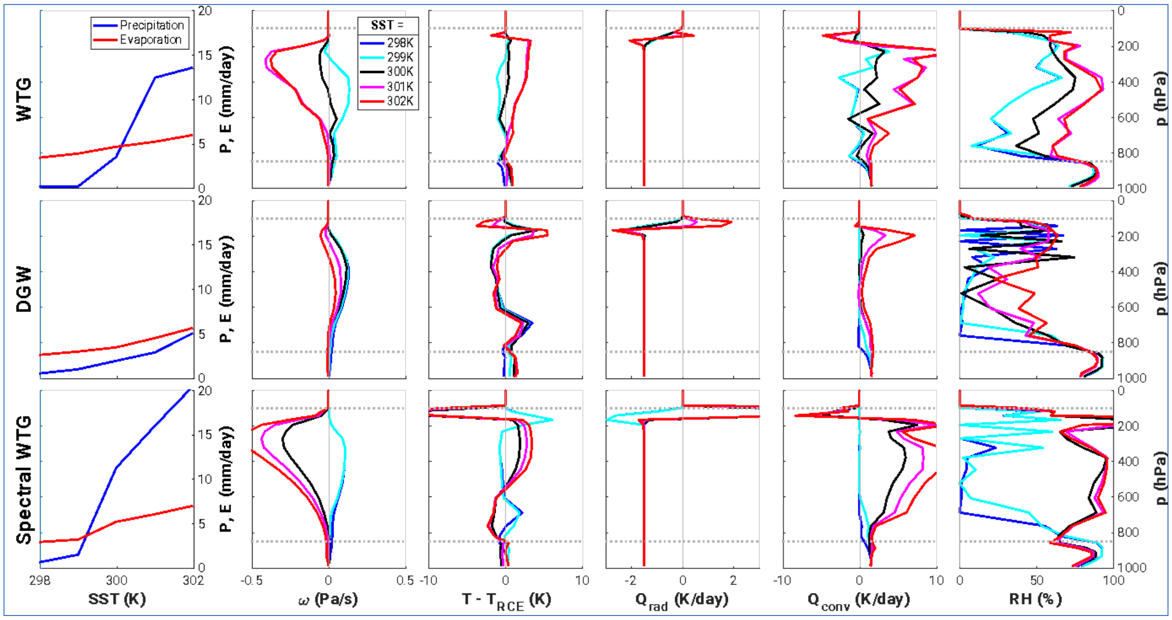

Figure 3. RsCi: Same as in Figure 2, but with τ_1 and τ set to nine hours and ϵ set to three days^{-1}.

If we increase the circulation parameters given in Daleu et al. (2016) even further to five times their original values (with τ_1 and τ set to fifteen hours and ϵ set to five days^{-1}), again leaving radiative and convective settings unmodified, the DGW method begins to yield heavy precipitation for higher SST (Figure 4). Thus, for this configuration, all methods behave qualitatively similarly, following the broad theoretical expectation that low SST will yield large-scale descent and low precipitation while high SST will yield large-scale ascent and heavy precipitation. However, the SST at which heavy precipitation begins to occur varies substantially from method to method, with this transition occurring at 300 K SST for the Spectral WTG method, 301 K SST for the WTG method, and 302 K SST for the DGW method. In addition, vertical velocity profiles tend to be more top-heavy for the WTG method and Spectral WTG method than for the DGW method, a difference also observed in Daleu et al. (2016) and Romps (2012). By design, vertical velocity profiles are smoother for the Spectral WTG and DGW methods than for the WTG method, since the second order wave equation in the DGW method and the mode-dependent damping in the Spectral WTG method allow temperature perturbations in the column to produce non-local responses in $\overline{\omega}$ (Herman and Raymond 2014, Wang et al. 2016, Kuang 2008). However, while these smoothing effects are observed in the convective heating profiles and the temperature deviation from RCE, they do not appear to smooth the column's relative humidity profile. This oscillatory structure of upper-tropospheric moisture is also observed in Hu et al. (2022), though this study focused on SCAM under RCE, not under parameterized large-scale dynamics. Nonetheless, the hypothesis posed in Hu et al. (2022) – that these oscillations in upper tropospheric moisture are caused by variations in convective height – is likely still relevant under parameterized large-scale dynamics at low SST.

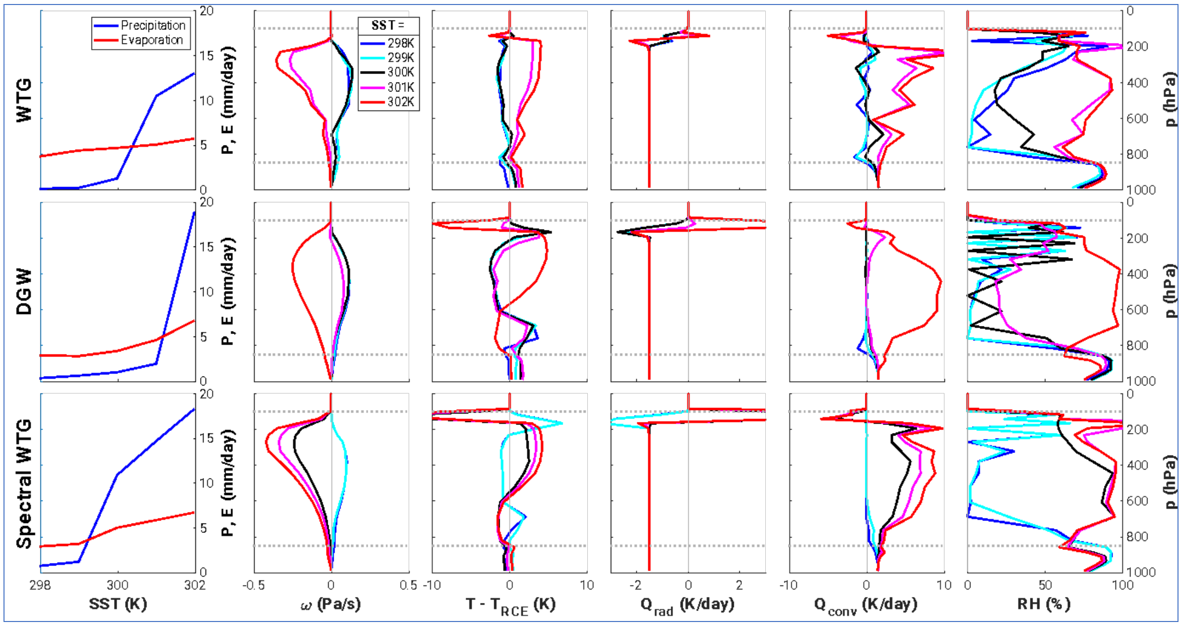

Figure 4. RsCi: Same as in Figures 2 and 3, but with τ_1 and τ set to fifteen hours and ϵ set to five days^{-1}.

The temperature deviation from the RCE reference profile tends to follow a similar structure across all methods. Temperature deviations across the mid troposphere are of opposite sign as the vertical velocity (in pressure coordinates, almost by design), with positive temperature anomalies being associated with large-scale ascent and negative temperature anomalies being associated with large-scale descent (Figure 4). However, in the upper and lower troposphere, we observe the opposite relationship: large-scale ascent is associated with negative temperature anomalies and large-scale descent is associated with positive temperature anomalies. In the upper troposphere, this reversal in the sign of the temperature deviation is likely caused by the inversion of the overall temperature profile. As shown in the RCE profiles (Figure 1), the temperature and potential temperature reach a local minimum at around 200 hPa, meaning that above this threshold large-scale ascent advects relatively low potential temperature air upward and large-scale descent advects relatively high potential temperature air downward. It is worth noting that the vertical velocity decays to zero at a lower altitude in the WTG method than in the DGW or the Spectral WTG method (Figure 4), meaning the upper-tropospheric temperature anomalies are also of smaller magnitude.

Next, we consider configurations with different radiative and convective settings, all using circulation parameters with five times the value given in Daleu et al. (2016). While all radiative and convective configurations were tested across a range of circulation parameters, all methods either performed nearly identically or substantially more in line with expectation for these larger values of circulation parameters (indicating weaker responses of the circulation to tropospheric temperature deviations from the target profile). To begin, we consider RsCu, where the number of tolerated negative buoyancy regions in the convective scheme (δ_{CIN}) is increased from one to three, but the radiation is still specified (Figure 5). In this case, all methods perform remarkably similarly to one another, transitioning from light to heavy precipitation at the same SST. Relative humidity and vertical velocity profiles also look remarkably similar across methods. However, in cases where deep convection does occur, convective ascent is generally weaker and the mid troposphere thus contains notably less moisture than it does for RsCi. These differences in the magnitude of the vertical velocity likely stem more from differences in the RCE reference profiles than from differences in the behavior of the convective scheme within the simulated column. Under less-inhibited convection settings (Cu), the RCE profile is more statically stable (Figure 1), meaning the free tropospheric temperature anomalies are smaller and the circulation is weaker (see Discussion for details).

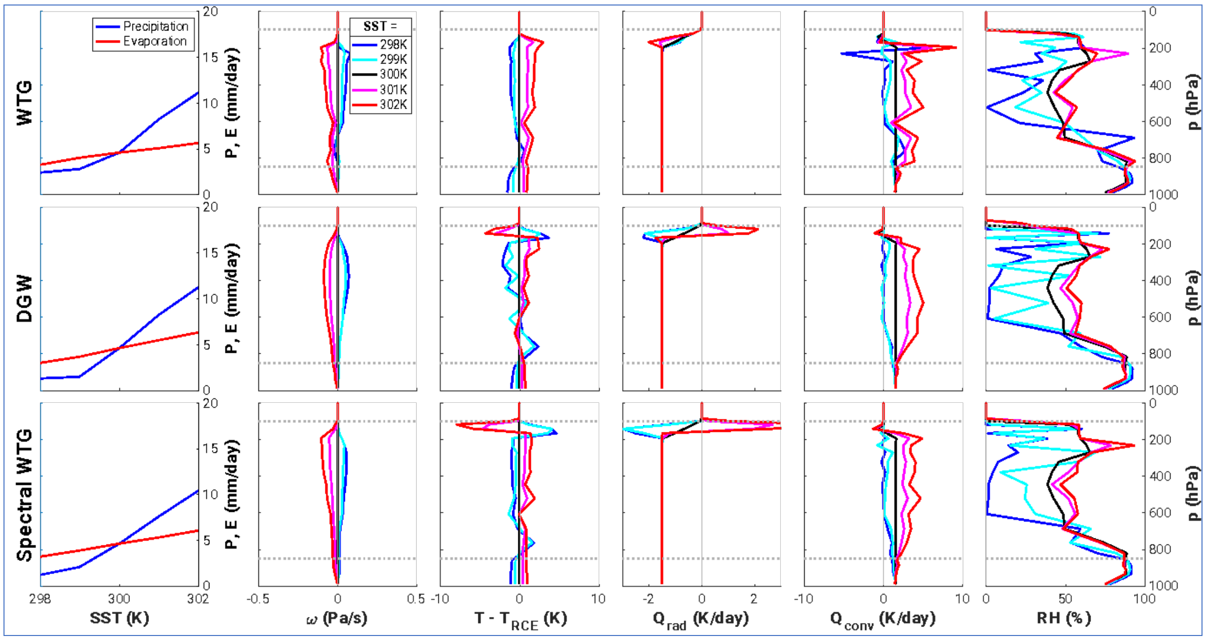

Figure 5. RsCu: Same as in Figure 4, but tolerating three levels of CIN in the convection scheme.

Next, we consider configurations using SCAM6's default interactive radiation scheme (RRTMG) rather than the idealized radiative cooling profile from Daleu et al. (2016). We present results for RiCi (Figure 6) and RiCu (Figure 7). Runs with lower SST tend to yield greater radiative cooling in the majority of the troposphere, primarily due to lower cloud fraction and thus reduced shortwave heating (not shown). As with the idealized radiation cases, using $\delta_{CIN} = 3$ tends to yield weaker convective ascent than using $\delta_{CIN} = 1$. However, this difference is smaller when using interactive radiation than when using specified radiation.

Sharp oscillations in convective heating suggest numerical issues in the 302 K SST run for the WTG method in Figure 7 (RiCu). In fact, while nearly all cases using circulation parameters with five times the value given in Daleu et al. (2016) performed reasonably, the WTG method performed somewhat strangely under interactive radiation and uninhibited convection. The expected monotonic relationship between SST and precipitation is apparent, but the method tends to favor deep convection; even at the lowest SST, large-scale descent is weaker than in the other methods, and correspondingly the troposphere does not as fully dry out.

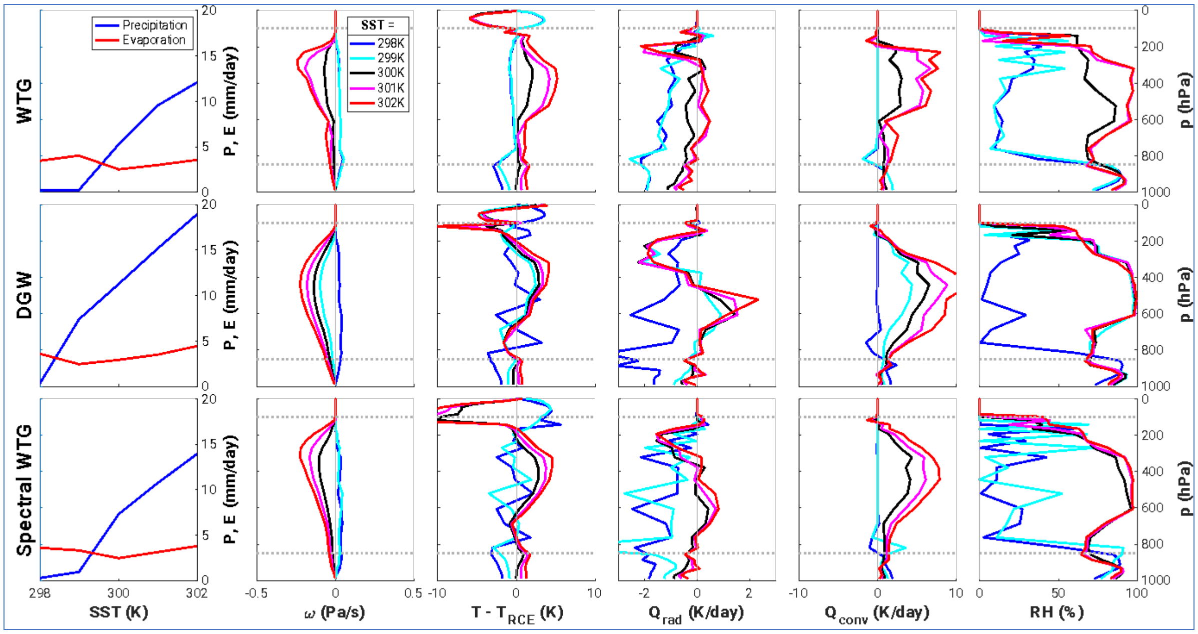

Figure 6. RiCi: Same as in Figure 4, but using interactive radiative cooling.

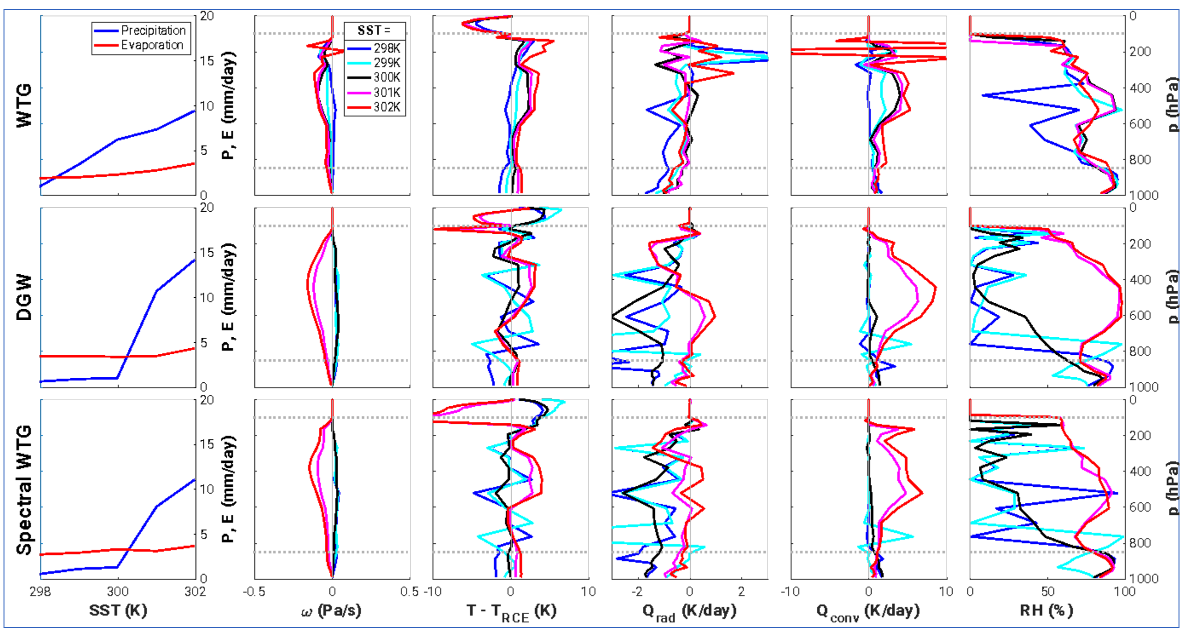

Figure 7. RiCu: Same as in Figure 5, but using interactive radiative cooling.

Finally, across configurations, there is significant variation in the "pickup" SST at which heavy precipitation begins to occur. Perhaps most notable in this regard is the DGW method: for RsCi (Figure 4) heavy precipitation begins to occur at an SST of 302 K, while for RiCi (Figure 6) this transition occurs at an SST of 299 K.

3.4 Comparison to GASS

One of the main goals of this study is to compare the performance of SCAM6 under parameterized large-scale dynamics to those of the models in the GASS Intercomparison Study

(Daleu et al. 2016). Figure 8 compares precipitation vs SST curves for the WTG, DGW, and Spectral WTG methods in SCAM6 (under idealized radiation and inhibited convection) to the range of values seen in SCMs and CRMs in Figure 3 of Daleu et al. (2016). For circulation parameters equal to those used in the GASS Intercomparison Study (dashed), the WTG and DGW methods are numerically unstable in SCAM6 and thus show no clear relationship between SST and precipitation. However, if key circulation parameters τ and ϵ are increased fivefold fifteen hours and five day^{-1} respectively (solid), the circulation response to a given free tropospheric temperature anomaly decreases and solutions become reasonably numerically resolved. These "relaxed" simulations produce the expected steep transition from light precipitation at low SST to heavy precipitation at high SST, and the simulations are quite comparable to the SCMs in Daleu at al. (2016).

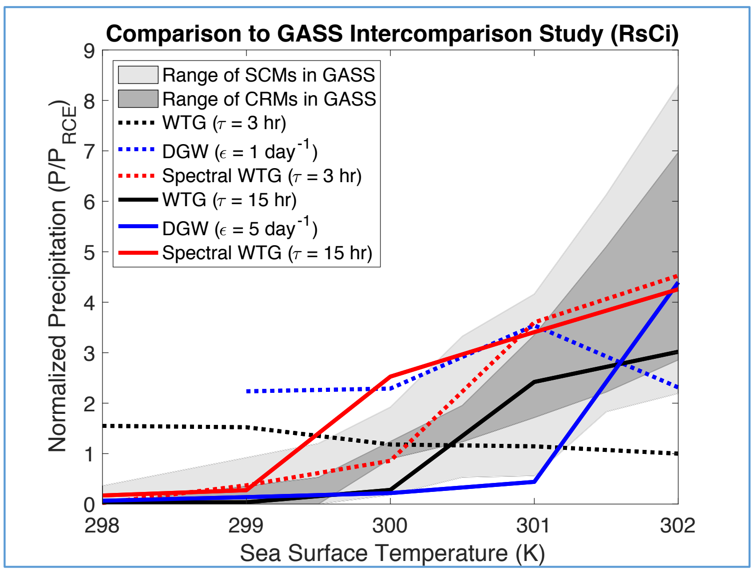

Figure 8. Normalized precipitation vs SST curves for the WTG, DGW, and Spectral WTG methods in SCAM6 under specified radiation and inhibited convection. Curves are shown for τ_1 and τ set to three hours and ϵ set to one day^{-1} (dashed) and for τ_1 and τ set to fifteen hours and ϵ set to five days^{-1} (solid). They are compared to the range of values seen in SCMs (light shading) and CRMs (dark shading) in Daleu et al. (2016).

3.5 Role of Static Stability Under Radiative-Convective Equilibrium

While each parameterization of large-scale dynamics performs slightly differently in a given configuration, the overall strength of the large-scale circulation (i.e., the magnitude of the vertical velocity profiles) remains roughly constant across all methods for given radiative and convective settings, allowing us to focus on the effect of modifying the radiation and convection schemes. Most notably in this regard, decreasing δ_{CIN} (Cu → Ci) tends to increase the strength of the circulation response, more so in the case of idealized radiation than in the case of interactive radiation.

At least under idealized radiation, the increase in circulation strength when δ_{CIN} is decreased can be explained by variations in the static stability of the RCE temperature profile from one configuration to another (Figure 9). In RCE under inhibited convection settings (Ci, $\delta_{CIN} = 1$), deep convection cannot grow as easily nor consume as much available instability (Hu et al.

2022). This results in a less statically stable tropospheric temperature profile than that under uninhibited convection settings (Cu, $\delta_{CIN} = 3$). However, at high SST (302 K) under parameterized large-scale dynamics, convection can grow deeply regardless of the convective settings. In this case, the balance in the temperature equation is between the convective heating and the vertical advection, since radiative cooling is much smaller than convective heating (Figures 4-5). If we assume that the convection scheme roughly acts to relax the column's temperature profile to an entraining moist adiabat set by the locally warm SST while the circulation acts to drive the column's temperature towards the RCE reference profile, then the steady-state solution in the column is effectively a time-averaged balance between these two forcings. Thus, if the RCE profile is less statically stable under inhibited convection settings (Ci), there will be a larger temperature difference between this RCE profile and the entraining moist adiabat towards which the convection scheme is relaxing (Figure 9). This larger temperature difference yields more large-scale ascent, more convection, and more steady-state precipitation. In other words, inhibited convection settings (Ci) create a less statically stable RCE profile that causes the circulation to introduce more CAPE into the column for a given circulation strength, yielding more convection and in turn a stronger compensating circulation. In addition, lower static stability in the column means that a larger vertical velocity is needed to create the same temperature tendency. Thus, even at low SST where convection is nearly absent, decreasing δ_{CIN} (Cu → Ci) increases the strength of the circulation, though it is of opposite sign. In these cases, the energetic balance is primarily between the radiation and the circulation, so a lower column static stability under Ci yields a stronger downward large-scale vertical velocity (Figures 4-5) even though the temperature deviation from RCE is similar (Figure 9).

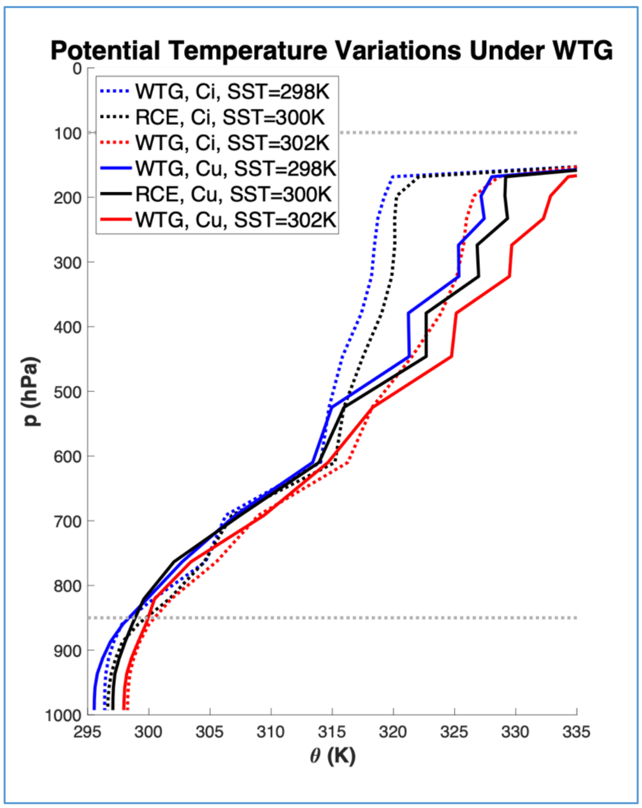

Figure 9. Time-averaged potential temperature profiles for RCE at 300 K SST (black), and WTG at 298 K SST (blue) and 302 K SST (red) for τ_1 and τ set to fifteen hours and ϵ set to five days^{-1} using a specified radiative cooling profile and tolerating either one (dashed) or three (solid) levels of CIN in the convection scheme.

We display this effect in Figure 9 for the WTG method; equivalent plots for the DGW and Spectral WTG methods are qualitatively similar (not shown). Under WTG, the time-averaged potential temperature profile at 302 K SST is much further from the RCE potential temperature profile for inhibited convection ($\delta_{CIN} = 1$, red dotted profile) than for uninhibited convection ($\delta_{CIN} = 3$, red solid profile). The RCE profile for CIN = 1 (black dotted) has substantially lower static stability than that for $\delta_{CIN} = 3$ (black solid), meaning there is a larger difference between the temperature profile towards which the convection scheme roughly drives the model (an entraining moist adiabat set by a 302 K fixed SST) and the RCE profile to which the circulation relaxes. This increased competition between the circulation and the convection scheme yields more steady-state precipitation and a stronger circulation response. At low SST, deep convection largely stops, making the balance primarily between the radiation and the circulation. Under specified radiation, radiative cooling is set to a constant 1.5 K day^{-1} in the bulk of the troposphere, so there are no changes in radiative effects that can cause different circulation strength for different convection parameters. However, the reduced slope of time-averaged potential temperature profile (static stability) means a larger vertical velocity is needed to create the same temperature tendency. Thus, increasing the barrier to convection strengthens both large-scale ascent and descent, but strengthens ascending motions more strongly.

How can we ensure the differences in circulation and precipitation described above are due to differences in the RCE reference states and not to the effect of δ_{CIN} on the convection directly? At high SST (302K), the time-average top of convection is near the top of the tropopause for all methods, regardless of the value of δ_{CIN} (not shown). However, in RCE, the top of convection is much lower for inhibited convection than for uninhibited convection. Since δ_{CIN} affects the convection scheme chiefly by setting the top of convection, this means that, at least in a time average sense, δ_{CIN} has a minimal effect on the column itself at high SST, and mostly affects the column through its modification to the RCE reference profile. These results are in line with findings from Hu et al. (2022).

We suggest that the above argument holds for interactive radiation cases as well. As in the specified radiation cases, increasing δ_{CIN} tends to increase the static stability of the reference RCE profile and decrease the precipitation and strength of the circulation response at high SST, but this effect is less extreme (Figure 10).

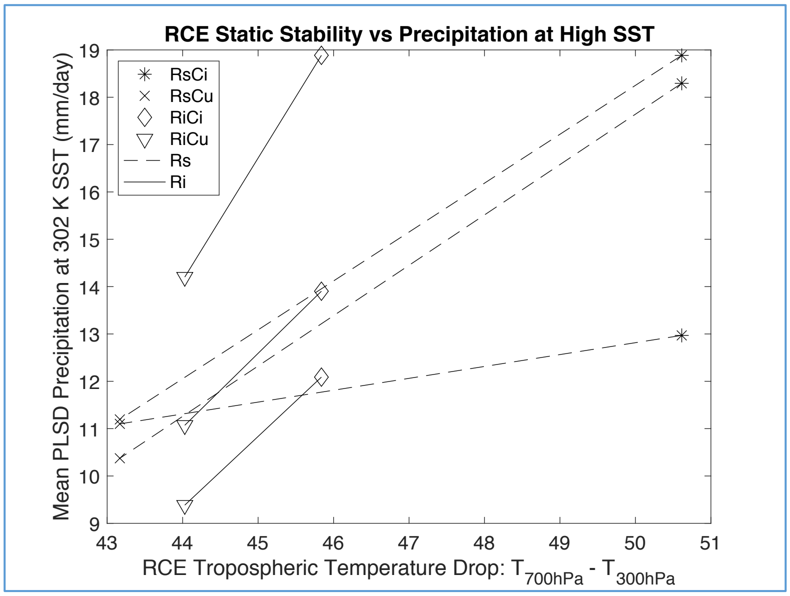

Figure 10. Mean precipitation at 302 K SST for all parameterized large-scale dynamics methods vs tropospheric temperature change (from 300 hPa to 700 hPa) in RCE. Higher tropospheric temperature change in RCE (at 300 K) indicates greater lapse rate and lower static stability in the RCE reference profile, causing greater time-averaged precipitation under parameterized large-scale dynamics at high SST (302 K). Lines, dashed and solid, indicate changes from Cu to Ci across individual methods (WTG, DGW, Spectral WTG).

Figure 10 shows the relationship between a bulk measure of RCE static stability and the 302 K SST precipitation under both idealized and modeled radiation. In both cases, precipitation at 302 K SST increases as the temperature drop from 700 to 300 hPa in the RCE reference state increases, i.e., the static stability decreases. While the change in static stability in RCE under interactive radiation is smaller than that under specified radiation, we observe the same qualitative effect on precipitation at this high relative SST. Moreover, the top of convection is again relatively independent of δ_{CIN} at high SST (not shown) and convective heating likewise dominates over radiative cooling, though the fact that radiation is interactive makes it more difficult to exclude the possibility that differences in radiative effects in the column itself play a role in setting the strength of the circulation response.

3.6 Relationship Between Humidity and Precipitation

Precipitation and column precipitable water vapor have been shown to be closely related in observations (e.g., Bretherton et al. 2004; Neelin et al. 2022) and the relationship between the two variables has been used as a diagnostic in prior modeling studies with parameterized large-scale dynamics (e.g., Wang and Sobel 2011). In Figure 11 we present the relationship between these variables under specified radiation (left panel) and interactive radiation (right panel). Precipitable water is known to be highly correlated to precipitation, with precipitation typically increasing steeply with precipitable water past a certain threshold. The WTG (blue), DGW (green), and Spectral WTG (black) methods qualitatively follow such expectations under all model configurations, though the methods can yield quantitatively different results depending on the radiative and convective settings. Under idealized radiation, all methods collapse onto a single curve for each convective setting. When convection is inhibited, precipitation spans a larger range of values and begins increasing steeply at a lower threshold of precipitable water. This is in line with our findings above, since we would expect a less statically stable RCE reference profile to yield larger precipitation at a given precipitable water. Under modeled radiation, the curves collapse substantially less overall, and separate more depending on the parameterization of large-scale dynamics than on the choice of convective settings. The WTG method yields the least precipitation at a given precipitable water, and the Spectral WTG method yields the most. This is likely due to the introduction of radiative-convective feedback, though it is unclear why each method interacts with the radiative scheme the specific way it does.

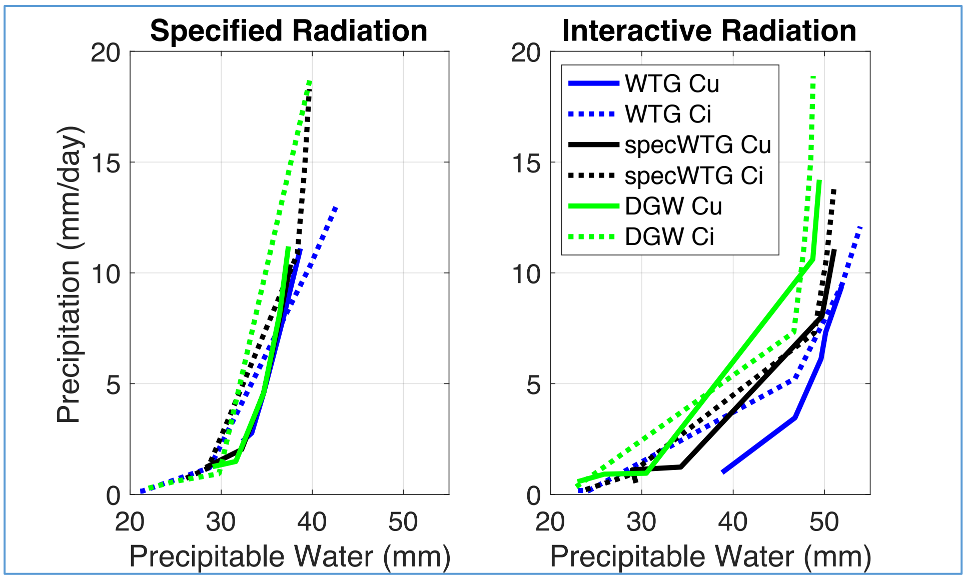

Figure 11. Precipitation vs precipitable water at all simulated SSTs for specified and interactive radiation. Results for both inhibited (Ci) and uninhibited convection (Cu) settings are shown.

4 Conclusions

This study has implemented various parameterizations of large-scale dynamics into NCAR's single column atmospheric model SCAM6, with the purpose of both furthering development of NCAR's Community Earth System Model and exploring the mechanisms that drive steady-state tropical precipitation.

All the parameterizations of large-scale dynamics considered here act to relax the column temperature towards a target profile, typically represented by a radiative-convective equilibrium (RCE) solution. We implemented three parameterizations of large-scale dynamics into SCAM6: the weak temperature gradient (WTG) method (Raymond and Zeng 2005), the damped gravity wave (DGW) method (Kuang 2011), and the spectral weak temperature gradient (Spectral WTG) method (Wang et al. 2016). These methods were run under the conditions used in the GASS Intercomparison Study (Daleu et al. 2015, 2016) and, once circulation parameters τ and ϵ were relaxed, under a variety of other convective and radiative settings: specified radiation with inhibited convection (RsCi), specified radiation with uninhibited convection (RsCu), interactive radiation with inhibited convection (RiCi), and interactive radiation with uninhibited convection (RiCu). With the target tropospheric temperature profile held fixed based on the relevant RCE solution (at 300 K SST), the underlying SST was varied, representing the effect of varying relative SST (e.g., as a function of position).

The WTG and DGW methods lead to erratic behavior, with indications of numerical instability, in SCAM6 with the values of τ and ϵ used in the GASS Intercomparison Study (Daleu et al. 2015, 2016). However, when these circulation parameters are increased fivefold, weakening the coupling between circulation and temperature, the WTG and DGW methods yield results qualitatively similar to those of Daleu et al. (2016), following the broad theoretical expectation that low SST will yield large-scale descent and low precipitation while high SST will yield large-scale ascent and heavy precipitation. As the radiation and convection schemes are modified, the WTG and DGW methods perform qualitatively similarly, but quantitatively differently, especially with regard to the SST at which the column transitions from low to high precipitation. The Spectral WTG method is more insensitive to changes in the circulation, radiation, and convection schemes, showing both greater numerical stability and a more consistent transition from light to heavy precipitation, always at the RCE SST or at an SST one K warmer.

For a given radiative and convective setting, all parameterizations of large-scale dynamics produce similar circulation strengths and precipitation levels to each other at very high and very low SST. However, across radiative and convective settings, circulation strength and precipitation level change substantially. Changing δ_{CIN} from one (inhibited convection) to three (uninhibited convection) weakens the circulation and reduces precipitation at high SST. We demonstrate that this change is driven primarily by an increase in the static stability of the RCE reference profile.

Future study is needed to ascertain the relevance of these results to CESM model development and to steady state tropical precipitation more broadly. Next steps might include running CESM with inhibited ($\delta_{CIN} = 1$) and uninhibited convection ($\delta_{CIN} = 3$) to see if the GCM replicates the changes to circulation strength and precipitation at high SST that we observe in SCAM6. Furthermore, if these changes are replicated, what effect do they have on climatological features in the tropics such as the intertropical convergence zone (ITCZ) and the Walker circulation? Does the static stability of the tropical average change with radiative forcing and is this associated with a change in the relationship between SST and precipitation?

While it is difficult to extrapolate from the simulations presented in this study, we can reasonably speculate that decreasing the barrier to convection (using $\delta_{CIN} = 3$ rather than $\delta_{CIN} = 1$) in CESM's convection scheme will yield a more realistic representation of tropical convection. Tropical temperature profiles tend to be broadly moist adiabatic, but the SCAM6 simulations using inhibited convection show sizable upper tropospheric deviations from a moist adiabat (Figure 9) due to the fact that the convection scheme predicts a chronically low convective cloud top. Using uninhibited convection seems to alleviate this problem and could potentially prevent CESM from overestimating tropical circulation strength. This appears to be in line with findings from previous studies (Xie et al. 2018, Wang and Zhang 2018, Hu et al. 2022). However, these predictions are speculative and should be explored in future research.

Similarly, it is still an open question why SCAM6 requires more relaxed circulation parameters than the SCMs considered in Daleu et al. (2016) for the WTG and DGW methods in order to behave well. Given the centrality of the deep convection scheme in setting the column's circulation and precipitation, it may be that the Zhang-McFarlane scheme (which is not used by any of the other SCMs in Daleu et al.) is more prone to runaway feedbacks when paired with the WTG and DGW methods. In any case, our results suggest that the Spectral WTG method's insensitivity to changes in radiation, convection, and circulation make it better suited to use in SCAM6 and model development for CESM.

Acknowledgments

This research was supported by National Science Foundation grant AGS-1933523. Isla Simpson and Andrew Gettelman were supported by the National Center for Atmospheric Research which is a major facility sponsored by the National Science Foundation under Cooperative Agreement 1852997. I-Kuan Hu is supported by the National Science Foundation (NSF) through Grant Number AGS-1839471.

Open Research

All presented data is available at https://zenodo.org/record/7999372.

References

[Bretherton et al. 2004] Bretherton, C. S., M. Peters, and L. Back, (2004). Relationships between water vapor path and precipitation over the tropical oceans. *Journal of Climate*, **17**, 1517–1528.

[Charney 1963] Charney, J. G., 1963: A note on large-scale motions in the tropics. *J. Atmos. Sci.*, **20**, 607-609.

[Daleu et al. 2012] Daleu, C., S. Woolnough, and R. Plant (2012). Cloud-resolving model simulations with one and two-way couplings via the weak-temperature gradient approximation, *J. Atmos. Sci*., **69**, 3683– 3699.

[Daleu et al. 2015] Daleu, C. L., S. J. Woolnough, R. S. Plant, S. Sessions, M. J. Herman, A. H. Sobel, S. Wang, D. Kim, A. Cheng, G. Bellon, P. Peyrille, F. Ferry, A. P. Siebesma, and B. van Ulft, (2015). Intercomparsion of methods of coupling between convection and large-scale circulation. part i: Comparison over uniform surface conditions. *J. Adv. Model. Earth Sys.,* **7**.

[Daleu et al. 2016] Daleu, C. L., S. J. Woolnough, R. S. Plant, S. Sessions, M. J. Herman, A. H. Sobel, S. Wang, D. Kim, A. Cheng, G. Bellon, P. Peyrille, F. Ferry, A. P. Siebesma, and B. van Ulft, (2015). Intercomparsion of methods of coupling between convection and large-scale circulation. part ii: Comparison over non-uniform surface conditions. *J. Adv. Model. Earth Sys*., **8**, 387-405.

[Danabasoglu et al. 2020] Danabasoglu, G., Lamarque, J. F., Bacmeister, J., Bailey, D. A., DuVivier, A. K., Edwards, J., Emmons, L. K., Fasullo, J., Garcia, R., Gettelman, A., Hannay, C., Holland, M. M., Large, W. G., Lauritzen, P. H., Lawrence, D. M., Lenaerts, J. T. M., Lindsay, K., Lipscomb, W. H., Mills, M. J., Neale, R., Oleson, K. W., Otto-Bliesner, B., Phillips, A. S., Sacks, W., Tilmes, S., Kampenhout, L., Vertenstein, M., Bertini, A., Dennis, J., Deser, C., Fischer, C., Fox-Kemper, B., Kay, J. E., Kinnison, D., Kushner, P. J., Larson, V. E., Long, M. C., Mickelson, S., Moore, J. K., Nienhouse, E., Polvani, L., Rasch, P. J., & Strand, W. G. (2020). The Community Earth System Model version 2 (CESM2). *J. Adv. Model. Earth Sys*., **7**.

[Gettelman et al. 2019] Gettelman, A., Truesdale, J. E., Bacmeister, J. T., Caldwell, P. M., Neale, R. B., Bogenschutz, P. A., & Simpson, I. R. (2019). The single column atmosphere model version 6 (SCAM6): Not a scam but a tool for model evaluation and development. *Journal of Advances in Modeling Earth Systems*, **11**(5), 1381– 1401.

[Golaz et al. 2002] Golaz, J.-C., Larson, V. E., & Cotton, W. R. (2002). A PDF-based model for boundary layer clouds. Part I: Method and model description. *Journal of the Atmospheric Sciences*, **59**(24), 3540– 3551.

[Held 2005] Held, I. (2005). The Gap between Simulation and Understanding in Climate Modeling. *Bulletin of the American Meteorological Society*, **86**, 1609-1614.

[Held et al. 1993] Held, I. M., R. S. Hemler, and V. Ramaswamy (1993). Radiative-convective equilibrium with explicit two-dimensional moist convection, *J. Atmos. Sci*., **50**, 3909– 3927.

[Herman and Raymond 2014] Herman, M., and D. Raymond (2014). WTG cloud modeling with spectral decomposition of heating. *J. Adv. Model. Earth Sys*., **6**, 1121-1140.

[Hu et al. 2022] Hu, I.-K., Mapes, B. E., Tulich, S. N., Neale, R. B., Gettelman, A., and Reed, K. A. (2022). Idealized simulations of the tropical climate and variability in the Single Column Atmosphere Model (SCAM): Radiative-convective equilibrium. *J. Adv. Model. Earth Syst.*, **14**, e2021MS002826.

[Jakob et al. 2019] Jakob, C., M. S. Singh, and L. Jungandreas (2019). Radiative convective equilibrium and organized convection: An observational perspective. *J. Geophys. Res. Atmos.*, **124**, 5418–5430.

[Kuang 2008] Kuang, Z. (2008). Modeling the interaction between cumulus convection and linear gravity waves using a limited-domain cloud system-resolving model, *J. Atmos. Sci.*, **65**, 576– 591.

[Kuang 2011] Kuang, Z. (2011). The wavelength dependence of the gross moist stability and the scale selection in the instability of column-integrated moist static energy, *J. Atmos. Sci*., **68**, 61– 74.

[Lacis et al. 1979] Lacis, A., W. C. Wang, and J. Hansen (1979). Correlated k-distribution method for radiative transfer in climate models: Applications to effect of cirrus clouds on climate. *NASA Conf. Publ*. **2076**, 309-314.

[Lindzen and Nigam 1987] Lindzen, R. S., and S. Nigam (1987). On the Role of Sea Surface Temperature Gradients in Forcing Low-Level Winds and Convergence in the Tropics. *J. Atmos. Sci.*, **44**, 2418–2436.

[Neelin et al. 2022] Neelin, J.D., C. Martinez-Villalobos, and S. Stechmann (2022). Precipitation Extremes and Water Vapor. *Curr. Clim. Change Rep*., **8**, 17–33.

[Raymond and Sessions 2007] Raymond, D., and S. Sessions (2007). Evolution of convection during tropical cyclogenesis, *Geophys. Res. Lett*., **34**, L06811.

[Raymond and Zeng 2005] Raymond, D. J., and X. Zeng (2005). Modeling tropical atmospheric convection in the context of the weak temperature gradient approximation. *Quart. J. Roy. Meteor. Soc*., **131**, 1301-1320.

[Romps 2012] Romps, David. (2012). Numerical Tests of the Weak Pressure Gradient Approximation. *J. Atmos. Sci*., **69**. 2846-2856.

[Sessions et al. 2010] Sessions, S., S. Sugaya, D. Raymond, and A. Sobel (2010). Multiple equilibria in a cloud-resolving model using the weak temperature gradient approximation, *J. Geophys. Res*., **115**, D12110.

[Sobel and Bellon 2009] Sobel, A., and G. Bellon (2009). The effect of imposed drying on parameterized deep convection, *J. Atmos. Sci*., **66**, 2085– 2096.

[Sobel and Bretherton 2000] Sobel, A. H., and C. S. Bretherton (2000). Modeling tropical precipitation in a single column. *J. Climate*, **13**, 4378–4392.

[Sobel et al. 2002] Sobel, A. H., I. M. Held, and C. S. Bretherton (2002). The ENSO signal in tropical tropospheric temperature. *J. Climate*, **15**, 2702–6.

[Sobel et al. 2007] Sobel, A., G. Bellon, and J. Bacmeister (2007). Multiple equilibria in a single-column model of the tropical atmosphere, *Geophys. Res. Lett*., **34**, L22804.

[Tompkins and Craig 1998] Tompkins, A., and G. Craig (1998). Radiative-convective equilibrium in a three-dimensional cloud-ensemble model, *Q. J. R. Meteorol. Soc*., **124**, 2073– 2097.

[Wang and Sobel 2011] Wang, S., and A. Sobel (2011). Response of convection to relative sea-surface temperature: Cloud-resolving simulations in two and three dimensions, *J. Geophys. Res*., **116**, D11119.

[Wang and Sobel 2012] Wang, S., and A. Sobel (2012). Impact of imposed drying on deep convection in a cloud-resolving model, *J. Geophys. Res*., **117**, D02112.

[Wang and Zhang 2018] Wang, M., and Zhang, G. J. (2018). Improving the Simulation of Tropical Convective Cloud-Top Heights in CAM5 with CloudSat Observations. *J. Climate*, **31**, 5189-5204.

[Wang et al. 2013] Wang, S., A. H. Sobel, and Z. Kuang (2013). Cloud-resolving simulation of TOGA-COARE using parameterized large-scale dynamics, *J. Geophys. Res*., **118**, 6290–6301.

[Wang et al. 2016] Wang, S., A. H. Sobel, and J. Nie (2016). Modeling the MJO in a cloud resolving model with parameterized large-scale dynamics: Vertical structure, radiation, and horizontal advection of dry air. *J. Adv. Model. Earth Syst*., **8**, 121–139.

[Xie et al. 2018] Xie, S., Lin, W., Rasch, P. J., Ma, P., Neale, R., Larson, V. E., et al. (2018). Understanding cloud and convective characteristics in version 1 of the E3SM atmosphere model. *J. Adv. Model. Earth Syst*., **10**(10), 2618–2644.

[Zhang and McFarlane 1995] Zhang, G. J., & McFarlane, N. A. (1995). Sensitivity of climate simulations to the parameterization of cumulus convection in the Canadian climate centre general circulation model. *Atmosphere-Ocean*, **33**(3), 407– 446.